

# Multiresolution Bilateral Filtering for Image Denoising

Ming Zhang and Bahadır K. Gunturk

**Abstract**—The bilateral filter is a nonlinear filter that does spatial averaging without smoothing edges; it has shown to be an effective image denoising technique. An important issue with the application of the bilateral filter is the selection of the filter parameters, which affect the results significantly. There are two main contributions of this paper. The first contribution is an empirical study of the optimal bilateral filter parameter selection in image denoising applications. The second contribution is an extension of the bilateral filter: multiresolution bilateral filter, where bilateral filtering is applied to the approximation (low-frequency) subbands of a signal decomposed using a wavelet filter bank. The multiresolution bilateral filter is combined with wavelet thresholding to form a new image denoising framework, which turns out to be very effective in eliminating noise in real noisy images. Experimental results with both simulated and real data are provided.

## I. INTRODUCTION

**T**HERE are different sources of noise in a digital image. Some noise components, such as the dark signal nonuniformity (DSNU) and the photoresponse nonuniformity (PRNU), display nonuniform spatial characteristics. This type of noise is often referred as fixed pattern noise (FPN) because the underlying spatial pattern is not time varying. Temporal noise, on the other hand, does not have a fixed spatial pattern. Dark current and photon shot noise, read noise, and reset noise are examples of temporal noise. The overall noise characteristics in an image depend on many factors, including sensor type, pixel dimensions, temperature, exposure time, and ISO speed. Noise is in general space varying and channel dependent. Blue channel is typically the noisiest channel due to the low transmittance of blue filters. In single-chip digital cameras, demosaicking algorithms are used to interpolate missing color components; hence, noise is not necessarily uncorrelated for different pixels. An often neglected characteristic of image noise is the spatial frequency. Referring to Fig. 1, noise may have low-frequency (coarse-grain) and high-frequency (fine-grain) fluctuations. High-frequency noise is relatively easier to remove; on



Fig. 1. Portion of an image captured with a Sony DCR-TRV27, and its red, green, and blue channels are shown in raster scan order. The blue channel is the most degraded channel; it has a coarse-grain noise characteristics. The red and green channels have fine-grain noise characteristics.

the other hand, it is difficult to distinguish between real signal and low-frequency noise.

Many denoising methods have been developed over the years; among these methods, wavelet thresholding is one of the most popular approaches. In wavelet thresholding, a signal is decomposed into its approximation (low-frequency) and detail (high-frequency) subbands; since most of the image information is concentrated in a few large coefficients, the detail subbands are processed with hard or soft thresholding operations. The critical task in wavelet thresholding is the threshold selection. Various threshold selection strategies have been proposed, for example, VisuShrink [1], SureShrink [2], and BayesShrink [3]. In the VisuShrink approach, a universal threshold that is a function of the noise variance and the number of samples is developed based on the minimax error measure. The threshold value in the SureShrink approach is optimal in terms of the Stein's unbiased risk estimator. The BayesShrink approach determines the threshold value in a Bayesian framework, through modeling the distribution of the wavelet coefficients as Gaussian. These shrinkage methods have later been improved by considering interscale and intrascale correlations of the wavelet coefficients [4]–[8]. The method in [4] models the neighborhoods of coefficients at adjacent positions and scales as Gaussian scale mixture and applies the Bayesian least squares estimation technique to update the wavelet coefficients. The method, known as the BLS-GSM method, is one of the benchmarks in the denoising literature due to its outstanding PSNR performance. Some recent methods have surpassed the PSNR performance of [4]. Among these methods, [9] constructs a global field of Gaussian scale mixtures to model subbands of wavelet coefficients as a product of two independent homogeneous Gaussian Markov random

Manuscript received December 10, 2007; revised August 20, 2008. Current version published November 12, 2008. This work was supported in part by the National Science Foundation under Grant 0528785 and in part by the National Institutes of Health under Grant 1R21AG032231-01. The associate editor coordinating the review of this manuscript and approving it for publication was Dr. Mario A. T. (G. E.) Figueiredo.

The authors are with the Department of Electrical and Computer Engineering, Louisiana State University, Baton Rouge, LA 70803 USA (e-mail: mzhang4@lsu.edu; bahadir@ece.lsu.edu).

Color versions of one or more of the figures in this paper are available online at <http://ieeexplore.ieee.org>.

Digital Object Identifier 10.1109/TIP.2008.2006658

fields, and develops an iterative denoising algorithm. [10]–[12] develop gray-scale and color image denoising algorithms based on sparse and redundant representations over learned dictionaries, where training and denoising use the K-SVD algorithm; [13] and [14] group 2-D image fragments into 3-D data arrays, and apply a collaborative filtering procedure, which consists of 3-D transformation, shrinkage of the transform spectrum, and inverse 3-D transformation. [15] models an ideal image patch as a linear combination of noisy image patches and formulates a total least squares estimation algorithm.

A recently popular denoising method is the bilateral filter [16]. While the term “bilateral filter” was coined in [16], variants of it have been published as the sigma filter [17], the neighborhood filter [18], and the SUSAN filter [19]. The bilateral filter takes a weighted sum of the pixels in a local neighborhood; the weights depend on both the spatial distance and the intensity distance. In this way, edges are preserved well while noise is averaged out. Mathematically, at a pixel location  $\mathbf{x}$ , the output of the bilateral filter is calculated as follows:

$$\tilde{I}(\mathbf{x}) = \frac{1}{C} \sum_{\mathbf{y} \in \mathcal{N}(\mathbf{x})} e^{-\frac{\|\mathbf{y}-\mathbf{x}\|^2}{2\sigma_d^2}} e^{-\frac{|I(\mathbf{y})-I(\mathbf{x})|^2}{2\sigma_r^2}} I(\mathbf{y}) \quad (1)$$

where  $\sigma_d$  and  $\sigma_r$  are parameters controlling the fall-off of the weights in spatial and intensity domains, respectively,  $\mathcal{N}(\mathbf{x})$  is a spatial neighborhood of  $\mathbf{x}$  and  $C$  is the normalization constant

$$C = \sum_{\mathbf{y} \in \mathcal{N}(\mathbf{x})} e^{-\frac{\|\mathbf{y}-\mathbf{x}\|^2}{2\sigma_d^2}} e^{-\frac{|I(\mathbf{y})-I(\mathbf{x})|^2}{2\sigma_r^2}}. \quad (2)$$

Although the bilateral filter was first proposed as an intuitive tool, recent papers have pointed out the connections with some well established techniques. In [20], it is shown that the bilateral filter is identical to the first iteration of the Jacobi algorithm (diagonal normalized steepest descent) with a specific cost function. [21] and [22] relate the bilateral filter with the anisotropic diffusion. The bilateral filter can also be viewed as an Euclidean approximation of the Beltrami flow, which produces a spectrum of image enhancement algorithms ranging from the  $L_2$  linear diffusion to the  $L_1$  nonlinear flows [23]–[25]. In [22], Buades *et al.* proposes a nonlocal means filter, where similarity of local patches is used in determining the pixel weights. When the patch size is reduced to one pixel, the nonlocal means filter becomes equivalent to the bilateral filter. [26] extends the work of [22] by controlling the neighborhood of each pixel adaptively.

In addition to image denoising, the bilateral filter has also been used in some other applications, including tone mapping [27], image enhancement [28], volumetric denoising [29], exposure correction [30], shape and detail enhancement from multiple images [31], and retinex [32]. [27] describes a fast implementation of the bilateral filter; the implementation is based on a piecewise-linear approximation in the intensity domain and appropriate sub-sampling in the spatial domain. [33] later derives an improved acceleration scheme for the filter through expressing it in a higher dimensional space where the signal intensity is added as the third dimension to the spatial domain.

Although the bilateral filter is being used more and more widely, there is not much theoretical basis on selecting the op-

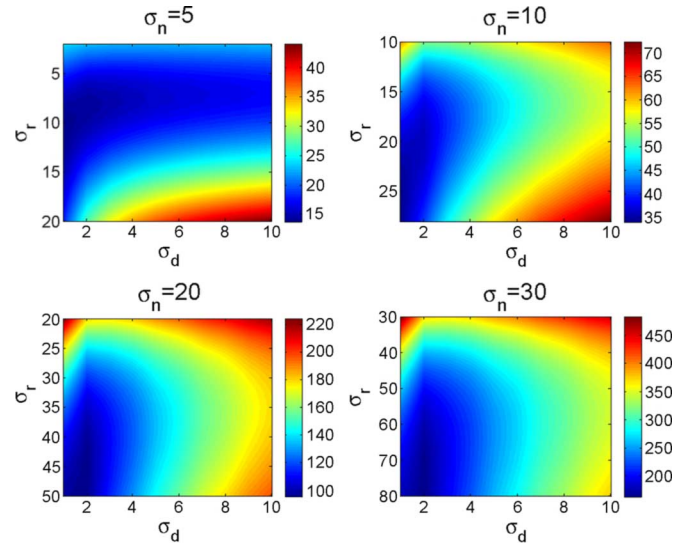


Fig. 2. MSE values between the original image and the denoised image for different values of  $\sigma_d$ ,  $\sigma_r$ , and the noise standard deviation  $\sigma_n$  are displayed. The results displayed are average results for 200 images. The number of samples along the  $\sigma_d$  (and  $\sigma_r$ ) direction is 10; the results are interpolated to produce smoother plots.

timal  $\sigma_d$  and  $\sigma_r$  values. These parameters are typically selected by trial and error. In Section II, we empirically analyze these parameters as a function of noise variance for image denoising applications. We will show that the value of  $\sigma_r$  is more critical than the value of  $\sigma_d$ ; we will in fact show that the optimal value of  $\sigma_r$  (in the mean square error sense) is linearly proportional to the standard deviation of the noise. In Section III, we will propose an extension of the bilateral filter. We will argue that the image denoising performance of the bilateral filter can be improved by incorporating it into a multiresolution framework. This will be demonstrated in Section IV with simulations and real data experiments.

## II. PARAMETER SELECTION FOR THE BILATERAL FILTER

There are two parameters that control the behavior of the bilateral filter. Referring to (1),  $\sigma_d$  and  $\sigma_r$  characterizes the spatial and intensity domain behaviors, respectively. In case of image denoising applications, the question of selecting optimal parameter values has not been answered completely from a theoretical perspective. [22] analyzes the behavior of the bilateral filter depending on the derivative of the input signal and  $\sigma_r/\sigma_d$  values. Conditions under which the filter behaves like a Gaussian filter, anisotropic filter, and shock filter were examined. [26] proposes an adaptive neighborhood size selection method for the nonlocal means algorithm, which can be considered as a generalization of the bilateral filter. The neighborhood size is chosen to minimize the upper bound of the local  $L_2$  risk; however, the effect of the intensity domain parameter is not considered. In this section, we provide an empirical study of optimal parameter values as a function of noise variance, and we will see that the intensity domain parameter  $\sigma_r$  is more critical than the spatial domain parameter  $\sigma_d$ .

To understand the relationship among  $\sigma_d$ ,  $\sigma_r$ , and the noise standard deviation  $\sigma_n$ , the following experiments were done.

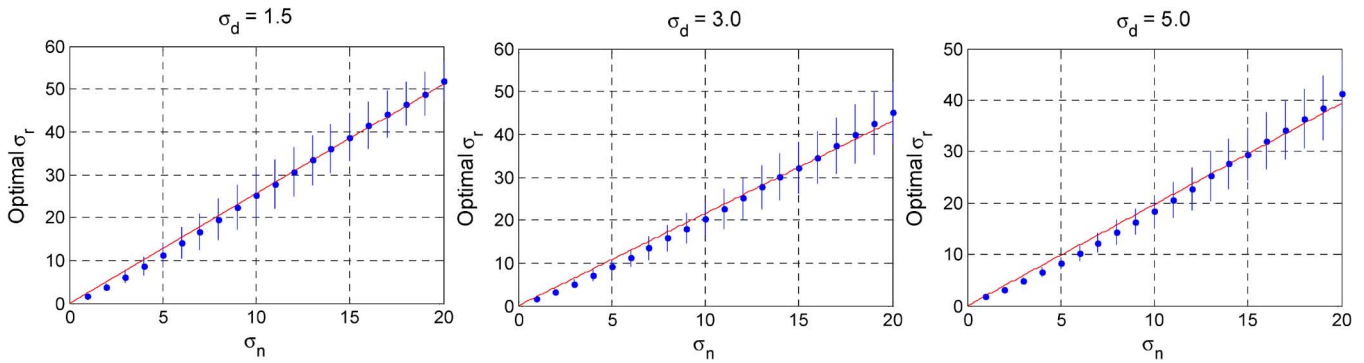


Fig. 3. Optimal  $\sigma_r$  values as a function of the noise standard deviation  $\sigma_n$  are plotted based on the experiments with 200 test images. The blue data points are the mean of optimal  $\sigma_r$  values that produce the smallest MSE for each  $\sigma_n$  value. The blue vertical lines denote the standard deviation of the optimal  $\sigma_r$  for the test images. The least squares fits to the means of the optimal  $\sigma_r/\sigma_n$  data are plotted as red lines. The slopes of these lines are, from left to right, 2.56, 2.16, and 1.97.

Zero-mean white Gaussian noise was added to some test images and the bilateral filter was applied for different values of the parameters  $\sigma_d$  and  $\sigma_r$ . The experiment was repeated for different noise variances and the mean squared error (MSE) values were recorded. The average MSE values are given in Fig. 2. Examining these plots, it can be seen that the optimal  $\sigma_d$  value is relatively insensitive to noise variance compared to the optimal  $\sigma_r$  value. It appears that a good range for the  $\sigma_d$  value is roughly [1.5–2.1]; on the other hand, the optimal  $\sigma_r$  value changes significantly as the noise standard deviation  $\sigma_n$  changes. This is an expected result because if  $\sigma_r$  is smaller than  $\sigma_n$ , noisy data could remain isolated and untouched as in the case of the salt-and-pepper noise problem of the bilateral filter [16]. When  $\sigma_r$  is sufficiently large,  $\sigma_d$  becomes important; apparently, increasing the value of  $\sigma_d$  too much results in over-smoothing and decrease of MSE.

To see the relationship between  $\sigma_n$  and the optimal  $\sigma_r$ , we set  $\sigma_d$  to some constant values, and determined the optimal  $\sigma_r$  values (minimizing MSE) as a function of  $\sigma_n$ . The experiments were again repeated for a set of images; the average values and the standard deviations are displayed in Fig. 3. We can make several observations from these plots. 1) Optimal  $\sigma_r$  and  $\sigma_n$  are linearly related to a large degree. 2) The standard deviation from the mean increases for larger values of  $\sigma_n$ . 3) When  $\sigma_d$  value is increased, the linearity between the optimal  $\sigma_r$  and  $\sigma_n$  still holds, but with lower slope. Obviously, there is no single value for  $(\sigma_r/\sigma_n)$  that is optimal for all images and  $\sigma_d$  values; in fact, future research should look for spatially adaptive parameter selection to take local texture characteristics into account. On the other hand, these experiments at least tell us some guidelines in selecting these parameters.

### III. A MULTIREOLUTION IMAGE DENOISING FRAMEWORK

As we have discussed in Section I, image noise is not necessarily white and may have different spatial frequency (fine-grain and coarse-grain) characteristics. Multiresolution analysis has been proven to be an important tool for eliminating noise in signals; it is possible to distinguish between noise and image information better at one resolution level than another. Images in Fig. 4 motivate the use of the bilateral filter in a multiresolution framework; in that figure, approximation subbands of a real noisy image are displayed. It is seen that the coarse-grain noise

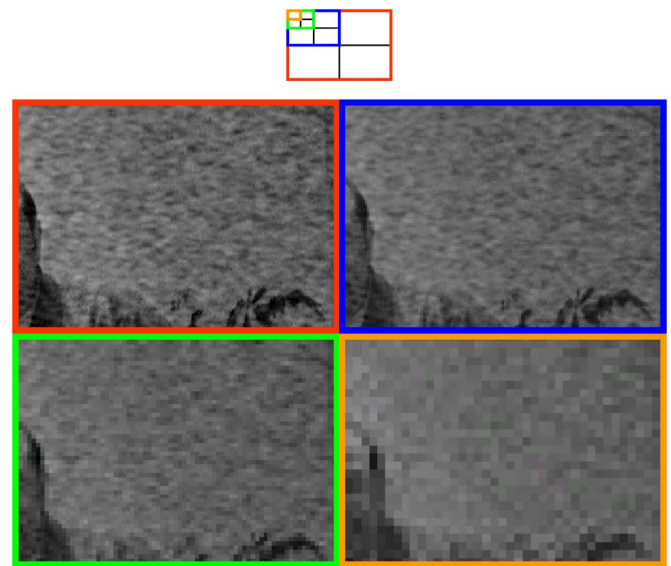


Fig. 4. Multiresolution characteristics of coarse-grain noise. A noisy image is decomposed into its frequency subbands using *db8* filters of Matlab. Part of the image is shown at the original resolution level and at three approximation subbands. The coarse-grain noise at the original level is difficult to identify and eliminate; the noise becomes fine grain as the image is decomposed, and can be eliminated more easily.

becomes fine-grain as the image is decomposed further into its subbands. While it is not possible to get rid of the coarse-grain noise at the highest level, it could be eliminated at a lower level.

The proposed framework is illustrated in Fig. 5: A signal is decomposed into its frequency subbands with wavelet decomposition; as the signal is reconstructed back, bilateral filtering is applied to the approximation subbands. Unlike the standard single-level bilateral filter [16], this multiresolution bilateral filter has the potential of eliminating low-frequency noise components. (This will become evident in our experiments with real data. Such an observation was also made in [34] for anisotropic diffusion, which has been shown to be related to the bilateral filter. Also, [31] utilizes the bilateral filter in a multiresolution scheme for shape and detail enhancement from multiple images.) Bilateral filtering works in approximation subbands; in addition, it is possible to apply wavelet thresholding to the detail subbands, where some noise components can be identified

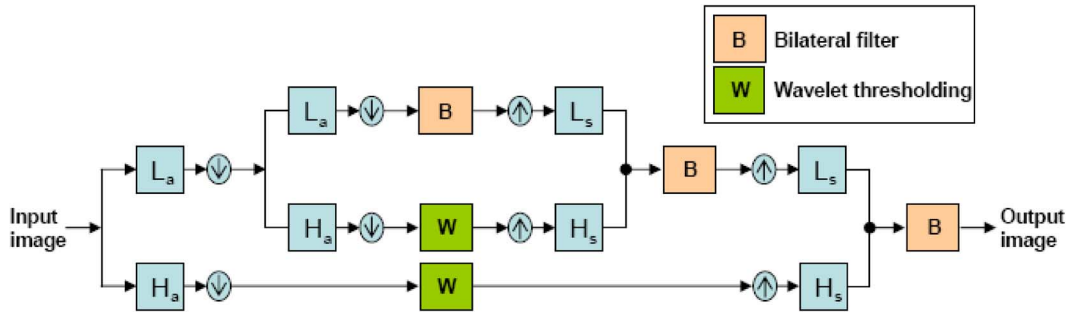


Fig. 5. Illustration of the proposed method. An input image is decomposed into its approximation and detail subbands through wavelet decomposition. As the image is reconstructed back, bilateral filtering is applied to the approximation subbands, and wavelet thresholding is applied to the detail subbands. The analysis and synthesis filters ( $L_a$ ,  $H_a$ ,  $L_s$ , and  $H_s$ ) form a perfect reconstruction filter bank. The illustration shows one approximation subband and one detail subband at each decomposition level; this would be the case when the data is 1-D. For a 2-D data, there are, in fact, one approximation and three (horizontal, vertical, and diagonal) detail subbands at each decomposition level. Also, in the illustration, there are two levels of decomposition; the approximation subbands could be decomposed further in an application.

TABLE I

PSNR COMPARISON OF THE BAYES SHRINK METHOD [3], THE BILATERAL FILTER [16], SEQUENTIAL APPLICATION OF THE BAYES SHRINK [3] AND THE BILATERAL FILTER [16] METHODS, NEW SURE THRESHOLDING [8], 3-D CF [14], AND THE PROPOSED METHOD FOR SIMULATED ADDITIVE WHITE GAUSSIAN NOISE OF VARIOUS STANDARD DEVIATIONS (THE NUMBERS WERE OBTAINED BY AVERAGING THE RESULTS OF SIX RUNS)

Input Image	$\sigma_n$	BayesShrink [3]	Bilateral Filter [16]	[3] Followed by [16]	New SURE [8]	3DCF [14]	Proposed Method
Barbara $512 \times 512$	10	31.25	31.37	30.92	32.18	34.98	31.79
	20	27.32	27.02	27.16	27.98	31.78	27.74
	30	25.34	24.69	25.23	25.83	29.81	25.61
Boats $512 \times 512$	10	31.98	32.02	31.81	32.90	33.92	32.58
	20	28.55	28.40	28.43	29.47	30.88	29.25
	30	26.71	26.57	26.66	27.63	29.12	27.24
Goldhill $512 \times 512$	10	31.94	32.08	31.93	32.69	33.62	32.48
	20	28.69	28.90	28.80	29.52	30.72	29.50
	30	27.13	27.50	27.34	27.89	29.16	27.77
Peppers $256 \times 256$	10	31.49	32.98	31.89	33.18	34.68	33.45
	20	27.85	29.07	28.01	29.33	31.29	30.20
	30	25.73	27.02	26.07	27.13	29.28	28.18
House $256 \times 256$	10	33.07	33.77	33.09	34.29	36.71	34.62
	20	29.83	29.63	29.79	30.93	33.77	31.37
	30	27.12	28.11	28.10	28.98	32.09	29.24
Lena $512 \times 512$	10	33.38	33.65	33.39	34.45	35.93	34.48
	20	30.27	30.33	30.29	31.33	33.05	31.28
	30	28.60	28.54	28.62	29.55	31.26	29.33
<b>Average</b>		29.24	29.54	29.31	30.29	32.34	30.34

and removed effectively. This new image denoising framework combines bilateral filtering and wavelet thresholding. In the next section, we will demonstrate that this framework produces results better than the individual applications of the wavelet thresholding or the bilateral filter, or successive application of the wavelet thresholding and the bilateral filter. We will also discuss the contribution of the wavelet thresholding to overall performance.

IV. EXPERIMENTS AND DISCUSSIONS

We have conducted some experiments to see the performance of the proposed framework quantitatively and visually. To do a

quantitative comparison, we simulated noisy images by adding white Gaussian noise with various standard deviations to some standard test images. These noisy images were then denoised using several algorithms and the PSNR results were calculated. For visual comparisons, real noisy images were used.

A. PSNR Comparison for Simulated Noisy Images

For each test image, three noisy versions were created by adding white Gaussian noise with standard deviations 10, 20, and 30. PSNR results for six methods are included in Table I.

TABLE II  
PSNR COMPARISON OF THE BAYES SHRINK METHOD [3], THE BILATERAL FILTER [16], 3-D CF [14], NEW SURE THRESHOLDING [8], BLS-GSM [4], AND THE PROPOSED METHOD FOR THE SPACE VARYING NOISE SIMULATION

Input Image	BayesShrink [3]	Bilateral Filter [16]	3DCF [14]	New SURE [8]	BLS-GSM [4]	Proposed Method
Barbara $512 \times 512$	31.9	32.2	34.3	24.0	29.7	32.6
Lena $512 \times 512$	33.1	33.4	35.2	22.7	31.2	34.1
Goldhill $512 \times 512$	32.2	32.6	32.3	23.6	29.9	32.8
Boat $512 \times 512$	32.5	32.6	32.9	23.6	30.3	32.9
House $256 \times 256$	32.5	33.4	35.8	22.7	31.4	34.1
Peppers $256 \times 256$	31.8	33.4	33.8	23.4	31.3	33.7
Average	32.3	32.9	34.0	23.3	30.6	33.4



(a)



(b)



(c)



(d)



(e)

Fig. 6. Comparison of the proposed method for different intensity distance measures and the number of decomposition levels. (a) Input image. (b) The distance measure is the Euclidean distance between (R,G,B) vectors. The number of decomposition levels is 2 for all channels. (c) The distance measure is the Euclidean distance between  $(L^*a^*b^*)$  vectors. The number of decomposition levels is 2 for all channels. (d) Each channel is denoised separately in  $L^*a^*b^*$  space. The number of decomposition levels is 1 for the  $L^*$  channel and 3 for the  $a^*$  and  $b^*$  channels. (e) The distance measure is the Euclidean distance between  $(L^*a^*b^*)$  vectors. The number of decomposition levels is 1 for the  $L^*$  channel and 3 for the  $a^*$  and  $b^*$  channels. In these experiments,  $\sigma_d = 3$ ,  $\sigma_r = 3 \times \sigma_n$ , and  $\sigma_n$  is estimated using the robust median estimator [3].

The first method is the BayesShrink wavelet thresholding algorithm [3]. Five decomposition levels were used; the noise vari-

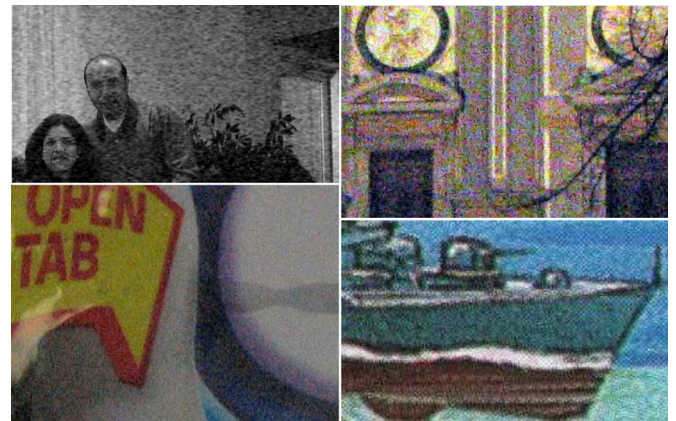


Fig. 7. Input images to be denoised using various algorithms. The top-left image is the blue channel of an image captured with Sony DCR-TRV27. The bottom-left image was captured with a Canon A530 at ISO 800. The other images were downloaded from [35].

ance was estimated using the robust median estimator [1]. The second method is the bilateral filter [16]. Based on our experiments discussed in the previous sections, we chose the following parameters for the bilateral filter:  $\sigma_d = 1.8$ ,  $\sigma_r = 2 \times \sigma_n$ , and the window size is  $11 \times 11$ . The third method is the sequential application of [3] and [16]. The reason this method was included is to see the combined effect of [3] and [16] and compare it with the proposed method. The fourth method is the new SURE method of [8]. It was recently published, and shown to produce very good results with nonredundant wavelet decomposition. The fifth method is the 3-D collaborative filtering (3-D CF) of [13], [14]. The sixth method is the proposed method. For the proposed method, *db8* filters in Matlab were used for one-level decomposition. For the bilateral filtering part of the proposed method, we set the parameters as follows:  $\sigma_d = 1.8$ , the window size is  $11 \times 11$ , and  $\sigma_r = 1.0 \times \sigma_n$  at each level. In case of the original bilateral filter,  $\sigma_r = 2 \times \sigma_n$  was a better choice. However, for the proposed method this lead to a smaller PSNR value on average. The reason is the double application of the bilateral filter in the proposed method. When  $\sigma_r$  was large, the images were smoothed to produce low PSNR values. After some experimentation,  $\sigma_r = 1.0 \times \sigma_n$  turned out to be a better choice in terms of PSNR values. Here, we should note that a higher PSNR does not necessarily correspond to a better visual quality (we will discuss this shortly). For the wavelet thresh-



Fig. 8. From top to bottom: Result of (a) the bilateral filter [16] with  $\sigma_d = 1.8$  and  $\sigma_r = 2 \times \sigma_n$ , (b) the 3-D CF method [14], (c) the proposed method with the number of decomposition levels is 4,  $\sigma_d = 1.8$ , and  $\sigma_r = 2 \times \sigma_n$  at each level, (d) the proposed method with the number of decomposition levels is 4,  $\sigma_d = 1.8$ , and  $\sigma_r = 3 \times \sigma_n$  at each level. The subband decomposition filters are *db8* in Matlab.

olding part of the proposed method, the BayesShrink method [3] was used; and the noise variance was estimated again with the robust median estimator technique. To eliminate the border effects, images were mirror-extended before the application of the bilateral filter and cropped to the original size at the end.

As seen in the PSNR results of Table I, the proposed method is 0.8 dB better than the original bilateral filter and 1.1 dB better than the BayesShrink method on average. The sequential application of [3] and [16] is only slightly better than [3] and worse

than [16]. Therefore, we conclude that the improvement of the proposed method is not due to the combined effect of [3] and [16], but due to the multiresolution application of the bilateral filter. While the new SURE method [8] is slightly worse than the proposed method, the 3-D CF method [14] is 2 dB better than the proposed method.

Most of the denoising methods are optimized for additive white Gaussian noise (AWGN); however, the real challenge is the performance for real noisy images. While we cannot quantitatively evaluate the performances for real noisy images, we may simulate spatially varying noise and make a quantitative comparison for it. This is more challenging than the AWGN case and could be a better representative of the performance for nonuniform noise situations. In our experiments, the space varying noise is generated by using a 2-D sinusoid of the same size as the input image; and the standard deviation of the noise at each pixel is controlled based on the amplitude of the sinusoid. To be specific, we generated the 2-D signal  $f(x_1, x_2) = (\sin(x_1/T)\sin(x_2/T) + 1)/2$ , where  $T$  is the period of the sinusoid. For an input image  $I(x_1, x_2)$ , the noisy image is  $I(x_1, x_2) + \sigma_d f(x_1, x_2)$ . The experiment was repeated for several standard test images (for  $T = 10$  and  $\sigma_d = 15$ ); the results are shown in Table II. Notice that methods specifically designed for additive white Gaussian noise do not perform well for this experiment. The neighborhood based denoising method of [14], which can be considered as an extension of the bilateral filter, is still the best; however, compared to the simulated AWGN noise experiments, the gap between the proposed method and [14] is much smaller. The standard bilateral filter also produces very good results. This experiment tells the effectiveness of the neighborhood based approach in case of space varying noise.

### B. Visual Comparison for Real Noisy Images

PSNR comparisons with simulated white Gaussian noise tell only a part of the story: First, it is well known that the PSNR is not a very good measure of visual quality; second, the white Gaussian noise assumption is not always accurate for real images. As a result, experiments with real data and visual inspections are necessary to evaluate the real performance of image denoising algorithms.

In case of color images, there is also the issue of what color space to use. To achieve good PSNR performance, the RGB space could be a good choice; however, for visual performance, it is a better idea to perform denoising in the perceptually uniform  $CIE - L^*a^*b^*$  color space. As humans find color noise more objectionable than luminance noise, stronger noise filtering could be applied to the color channels  $a^*$  and  $b^*$  compared to the luminance channel  $L^*$  without making the image visually blurry. Fig. 6 provides results of the proposed method for the RGB and the  $L^*a^*b^*$  spaces. For the RGB space result [Fig. 6(b)], the Euclidean distance between the (R,G,B) vectors is used as the intensity domain distance measure, and two levels of decomposition is applied to each channel. A close examination reveals that coarse-grain color artifacts are visible especially on the facial and hand regions. Fig. 6(c) is the result when the Euclidean distance between the  $(L^*, a^*, b^*)$  vectors is used, and again two levels of decomposition is applied to each

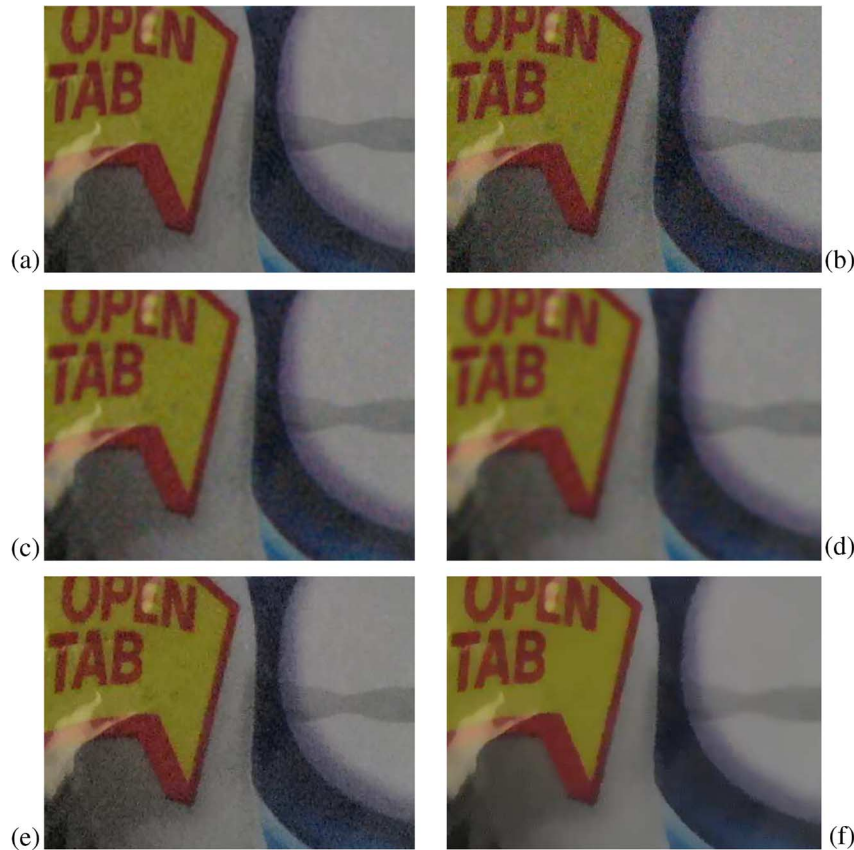


Fig. 9. (a) Result of the 3-D CF method [14]. (b) The bilateral filter [16] with  $\sigma_d = 1.8$  and  $\sigma_r = 3 \times \sigma_n$ . (c) The bilateral filter [16] with  $\sigma_d = 1.8$  and  $\sigma_r = 20 \times \sigma_n$ . (d) The bilateral filter [16] with  $\sigma_d = 5.0$  and  $\sigma_r = 20 \times \sigma_n$ . (e) The proposed method with the number of decomposition levels is (1,4,4) for the  $(L^*, a^*, b^*)$  channels, respectively. That is, the  $L^*$  channel is decomposed one level, and  $a^*$  and  $b^*$  channels are decomposed four levels. (f) The proposed method with the number of decomposition levels is (2,4,4) for the  $(L^*, a^*, b^*)$  channels, respectively. For the proposed method,  $\sigma_d = 1.8$ , and  $\sigma_r = 3 \times \sigma_n$  at each level. The subband decomposition filters are *db8* in Matlab. The noise parameter  $\sigma_n$  is estimated using the robust median estimator.

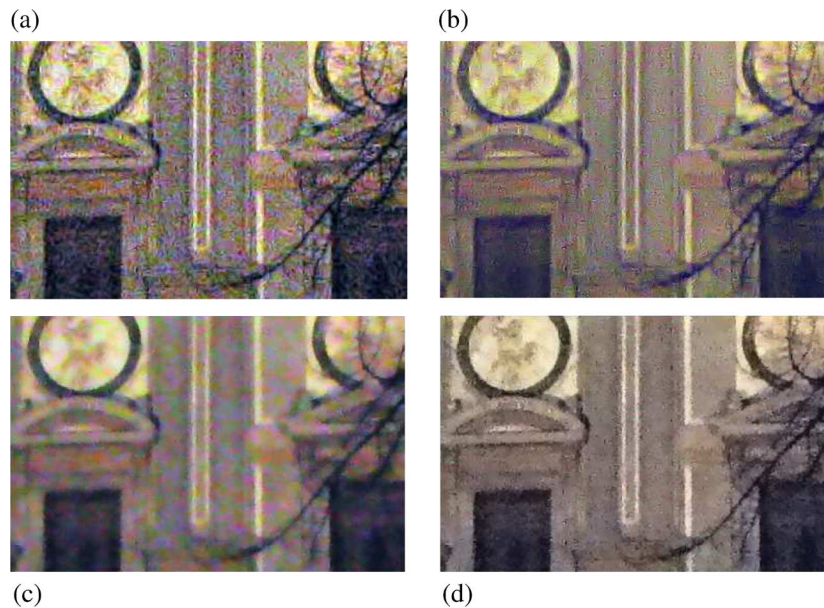


Fig. 10. (a) Result of the 3-D CF method [14]. (b) The BLS-GSM result obtained from [35]. (c) The bilateral filter [16] result. (d) Result of the proposed method. For the bilateral filter,  $\sigma_d = 1.8$ ,  $\sigma_r = 10 \times \sigma_n$ , and the window size is  $11 \times 11$ . For the proposed method,  $\sigma_d = 1.8$ ,  $\sigma_r = 3 \times \sigma_n$  at each level, the window size is  $11 \times 11$ , and the number of decomposition levels is (1,4,4) for the  $(L^*, a^*, b^*)$  channels, respectively. The wavelet filters are *db8* in Matlab. The noise parameter  $\sigma_n$  is estimated using the robust median estimator.

channel. The results in Fig. 6(b) and (c) are very similar. Fig. 6(d) is the result when each channel is treated separately, and when the number of decomposition levels is 1, 3, and 3

for  $L^*$ ,  $a^*$ , and  $b^*$  channels, respectively. Fig. 6(e) is the result when the Euclidean distance between the  $(L^*, a^*, b^*)$  vectors is used, and when the number of decomposition levels is 1, 3,

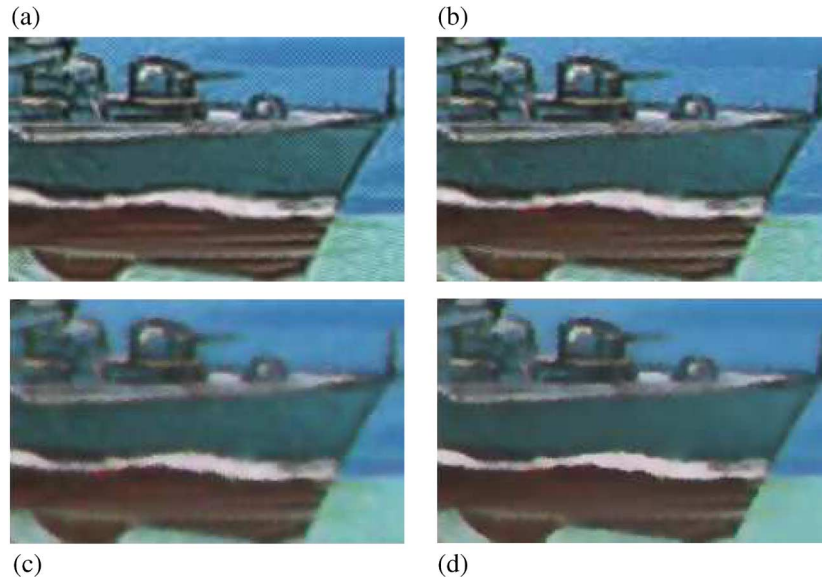


Fig. 11. (a) Result of the 3-D CF method [14]. (b) The BLS-GSM result obtained from [35]. (c) The bilateral filter [16] result. (d) Result of the proposed method. For the bilateral filter,  $\sigma_d = 1.8$ ,  $\sigma_r = 10 \times \sigma_n$ , and the window size is  $11 \times 11$ . For the proposed method,  $\sigma_d = 1.8$ ,  $\sigma_r = 3 \times \sigma_n$  at each level, the window size is  $11 \times 11$ , and the number of decomposition levels is (1,4,4) for the  $(L^*, a^*, b^*)$  channels, respectively. The wavelet filters are *db8* in Matlab. The noise parameter  $\sigma_n$  is estimated using the robust median estimator.

and 3 for  $L^*$ ,  $a^*$ , and  $b^*$  channels, respectively. Notice that in Fig. 6(d) and (e), texture is better preserved and coarse-grain noise is better eliminated compared to the previous results. Among the last two, there is not much observable difference. As a result, for perceptual reasons, we advocate applying and optimizing the denoising algorithms in the  $L^*a^*b^*$  space.

Next, we show a set of results for real noisy images. In all these experiments,  $\sigma_d$  and  $\sigma_r$  parameters fixed at  $\sigma_d = 1.8$  and  $\sigma_r = 3 \times \sigma_n$  produced very good results for the proposed method ( $\sigma_n$  was estimated using the robust median estimator [3] for all images). Therefore, we can claim that the proposed method is data-driven and robust for good visual performance.

Fig. 7 shows four test images. The first image is the blue channel of an image captured with Sony DCR-TRV27. The second image was captured with a Canon A530 at ISO 800. The other images were downloaded from [35].

In Fig. 8, we compare the standard bilateral filter, the 3-D CF method [14], and the proposed method. The input image was corrupted significantly with coarse-grain noise. The results show that the standard bilateral filter and the 3-D CF method are not effective against the coarse-grain noise. We provide two results for the proposed method.  $\sigma_r = 2 \times \sigma_n$  for one result; and  $\sigma_r = 3 \times \sigma_n$  for the other. The coarse grain noise is reduced significantly in both cases. While more noise components are eliminated for larger  $\sigma_r$ , contouring artifacts may start to appear, which is a common problem of the bilateral filtering and anisotropic diffusion.

In Fig. 9, we compare the 3-D CF method [14], the standard bilateral filter and the proposed method. The standard bilateral filter was tested for various values of  $\sigma_d$  and  $\sigma_r$ . Some representative results are shown. As seen in Fig. 9(b)–(d), no matter what parameter values are chosen for the standard bilateral filter, the coarse-grain chroma noise could not be eliminated effectively (we have also tested the iterative application of the bilat-

eral filter; the results were not good either, and were not included in the figure). Two results obtained by the proposed method are given: For the result in Fig. 9(e), the number of decomposition levels for the luminance channel is one; and in Fig. 9(f) it is two. For both results, the number of decomposition levels for the chrominance channels is four. Coarse-grain chroma noise is eliminated in both cases. Increasing the number of decomposition levels for the luminance channel produces a smoother image as seen in Fig. 9(f).

In Figs. 10 and 11, results of the 3-D CF method [14], the BLS-GSM method [4], the bilateral filter [16], and the proposed method are presented for real images provided at [35]. Among these methods, the proposed method is apparently producing more visually pleasing results than the others. Notice the lack of color in Fig. 10 for the proposed method; this is due to the higher number of decomposition levels for the chrominance channels. If the number of decomposition levels is reduced, the result would be more colorful. In Fig. 11, noise was not completely eliminated by the 3-D CF or the BLS-GSM methods. The result of the bilateral filter is less noisy but overly smoothed. The result of the proposed method can be considered as the best visual one among three.

Finally, we should comment on the contribution of the wavelet thresholding to the multiresolution framework (as mentioned earlier, in our experiments, we used the BayesShrink method [3] for the wavelet thresholding part). We have done experiments with and without the wavelet thresholding. For real image experiments, the difference is barely visible. That is, the dominant contribution is coming from the multiresolution bilateral filtering, and the contribution of wavelet thresholding is little. On the other hand, in additive white Gaussian noise simulations, wavelet thresholding has resulted in an improvement of about 0.5 dB in PSNR. Considering all aspects, we did not want to exclude wavelet thresholding from the proposed

framework because another wavelet thresholding method could produce better results, and we leave the investigation of this as a future work.

## V. CONCLUSION

In this paper, we make an empirical study of the optimal parameter values for the bilateral filter in image denoising applications and present a multiresolution image denoising framework, which integrates bilateral filtering and wavelet thresholding. In this framework, we decompose an image into low- and high-frequency components, and apply bilateral filtering on the approximation subbands and wavelet thresholding on the detail subbands. We have found that the optimal  $\sigma_r$  value of the bilateral filter is linearly proportional to the standard deviation of the noise. The optimal value of the  $\sigma_d$  is relatively independent of the noise power. Based on these results, we estimate the noise standard deviation at each level of the subband decomposition and use a constant multiple of it for the  $\sigma_r$  value of bilateral filtering. The experiments with real data demonstrate the effectiveness of the proposed method.

Note that in all real image experiments,  $\sigma_n$  values were estimated from the data, and the same  $\sigma_d$  and  $(\sigma_r/\sigma_n)$  values produced satisfactorily good results for the proposed method. That is, once the parameters were decided, there was no need to re-adjust them for another image.

The key factor in the performance of the proposed method is the multiresolution application of the bilateral filter. It helped eliminating the coarse-grain noise in images. The wavelet thresholding adds power the proposed method as some noise components can be eliminated better in detail subbands. We used a specific wavelet thresholding technique (i.e., the BayesShrink method); it is possible to improve the results further by using better detail-subband-denoising techniques or using redundant wavelet decomposition. These issues and the detailed analysis of parameter selection for the proposed framework are left as future work. We believe that the proposed framework will inspire further research towards understanding and eliminating noise in real images and help better understanding of the bilateral filter.

## REFERENCES

- [1] D. L. Donoho and I. M. Johnstone, "Ideal spatial adaptation by wavelet shrinkage," *Biometrika*, vol. 81, no. 3, pp. 425–455, 1994.
- [2] D. L. Donoho, I. M. Johnstone, G. Kerkycharian, and D. Picard, "Wavelet shrinkage: Asymptopia?," *J. Roy. Statist. Assoc. B*, vol. 57, no. 2, pp. 301–369, 1995.
- [3] S. G. Chang, B. Yu, and M. Vetterli, "Adaptive wavelet thresholding for image denoising and compression," *IEEE Trans. Image Process.*, vol. 9, no. 9, pp. 1532–1546, Sep. 2000.
- [4] J. Portilla, V. Strela, M. J. Wainwright, and E. P. Simoncelli, "Image denoising using scale mixtures of gaussians in the wavelet domain," *IEEE Trans. Image Process.*, vol. 12, no. 11, pp. 1338–1351, Nov. 2003.
- [5] A. Pizurica and W. Philips, "Estimating the probability of the presence of a signal of interest in multiresolution single- and multiband image denoising," *IEEE Trans. Image Process.*, vol. 15, no. 3, pp. 654–665, Mar. 2006.
- [6] L. Sendur and I. W. Selesnick, "Bivariate shrinkage functions for wavelet-based denoising exploiting interscale dependency," *IEEE Trans. Signal Process.*, vol. 50, no. 11, pp. 2744–2756, Nov. 2002.
- [7] L. Sendur and I. W. Selesnick, "Bivariate shrinkage with local variance estimation," *IEEE Signal Process. Lett.*, vol. 9, no. 12, pp. 438–441, Dec. 2002.
- [8] F. Luisier, T. Blu, and M. Unser, "A new sure approach to image denoising: Inter-scale orthonormal wavelet thresholding," *IEEE Trans. Image Process.*, vol. 16, no. 3, pp. 593–606, Mar. 2007.
- [9] S. Lyu and E. P. Simoncelli, "Statistical modeling of images with fields of gaussian scale mixtures," in *Advances in Neural Information Processing Systems 19*, B. Schölkopf, J. Platt, and T. Hoffman, Eds. Cambridge, MA: MIT Press, 2007, pp. 945–952.
- [10] M. Elad and M. Aharon, "Image denoising via learned dictionaries and sparse representation," presented at the IEEE Computer Vision and Pattern Recognition, Jun. 2006.
- [11] M. Elad and M. Aharon, "Image denoising via sparse and redundant representations over learned dictionaries," *IEEE Trans. Image Process.*, vol. 15, no. 12, pp. 3736–3745, Dec. 2006.
- [12] J. Mairal, M. Elad, and G. Sapiro, "Sparse representation for color image restoration," *IEEE Trans. Image Process.*, vol. 17, no. 1, pp. 53–69, Jan. 2008.
- [13] K. Dabov, V. Katkovnik, A. Foi, and K. Egiazarian, "Image denoising with block-matching and 3D filtering," presented at the SPIE Electronic Imaging: Algorithms and Systems V, Jan. 2006.
- [14] K. Dabov, A. Foi, V. Katkovnik, and K. Egiazarian, "Image denoising by sparse 3D transform-domain collaborative filtering," *IEEE Trans. Image Process.*, vol. 16, no. 8, pp. 2080–2095, Aug. 2007.
- [15] K. Hirakawa and T. W. Parks, "Image denoising using total least squares," *IEEE Trans. Image Process.*, vol. 15, no. 9, pp. 2730–2742, Sep. 2006.
- [16] C. Tomasi and R. Manduchi, "Bilateral filtering for gray and color images," in *Proc. Int. Conf. Computer Vision*, 1998, pp. 839–846.
- [17] J. S. Lee, "Digital image smoothing and the sigma filter," *CVGIP: Graph. Models and Image Process.*, vol. 24, no. 2, pp. 255–269, Nov. 1983.
- [18] L. Yaroslavsky, *Digital Picture Processing—An Introduction*. New York: Springer Verlag, 1985.
- [19] S. M. Smith and J. M. Brady, "Susan—A new approach to low level image processing," *Int. J. Comput. Vis.*, vol. 23, pp. 45–78, 1997.
- [20] M. Elad, "On the origin of the bilateral filter and ways to improve it," *IEEE Trans. Image Process.*, vol. 11, no. 10, pp. 1141–1151, Oct. 2002.
- [21] D. Barash, "A fundamental relationship between bilateral filtering, adaptive smoothing, and the nonlinear diffusion equation," *IEEE Trans. Pattern Anal. Mach. Intell.*, vol. 24, no. 6, pp. 844–847, Jun. 2002.
- [22] A. Buades, B. Coll, and J. Morel, "Neighborhood filters and PDE's," *Numer. Math.*, vol. 105, pp. 1–34, 2006.
- [23] N. Sochen, R. Kimmel, and R. Malladi, "A general framework for low level vision," *IEEE Trans. Image Process.*, vol. 7, no. 3, pp. 310–318, Mar. 1998.
- [24] N. Sochen, R. Kimmel, and A. M. Bruckstein, "Diffusions and confusions in signal and image processing," *J. Math. Imag. Vis.*, vol. 14, no. 3, pp. 195–209, 2001.
- [25] A. Spira, R. Kimmel, and N. Sochen, "A short time beltrami kernel for smoothing images and manifolds," *IEEE Trans. Image Process.*, vol. 16, no. 6, pp. 1628–1636, Jun. 2007.
- [26] C. Kervrann and J. Boulanger, "Optimal spatial adaptation for patch-based image denoising," *IEEE Trans. Image Process.*, vol. 15, no. 10, pp. 2866–2878, Oct. 2006.
- [27] F. Durand and J. Dorsey, "Fast bilateral filtering for the display of high-dynamic-range images," in *Proc. SIGGRAPH*, 2002, pp. 257–266.
- [28] E. Eisemann and F. Durand, "Flash photography enhancement via intrinsic relighting," in *Proc. SIGGRAPH*, 2004, pp. 673–678.
- [29] W. C. K. Wong, A. C. S. Chung, and S. C. H. Yu, "Trilateral filtering for biomedical images," in *Proc. IEEE Int. Symp. Biomedical Imaging*, 2004, pp. 820–823.
- [30] E. P. Bennett and L. McMillan, "Video enhancement using per-pixel virtual exposures," *ACM Trans. Graph.*, vol. 24, no. 3, pp. 845–852, 2005.
- [31] R. Fattal, M. Agrawala, and S. Rusinkiewicz, "Multiscale shape and detail enhancement from multi-light image collections," *ACM Trans. Graph.*, vol. 26, no. 3, Aug. 2007.
- [32] M. Elad, "Retinex by two bilateral filters," *Scale-Space, Lecture Notes in Comput. Sci.*, pp. 7–10, Apr. 2005.
- [33] S. Paris and F. Durand, "A fast approximation of the bilateral filter using a signal processing approach," in *Proc. Eur. Conf. Computer Vision*, 2006, pp. 568–580.
- [34] S. Acton, "Multigrid anisotropic diffusion," *IEEE Trans. Image Process.*, vol. 7, no. 3, pp. 280–291, Mar. 1998.
- [35] Color Test Images [Online]. Available: <http://decsai.ugr.es/~javier/denoise> April 2008



**Ming Zhang** was born in 1984. He received the B.S. degree in information engineering from Beijing University of Posts and Telecommunications (BUPT), China, in 2006. He is currently pursuing the M.S. degree at Louisiana State University, Baton Rouge.

His main research interests are in image denoising, blocking artifacts reduction, and high dynamic range imaging.



**Bahadir K. Gunturk** received the B.S. degree in electrical engineering from Bilkent University, Turkey, in 1999, and the M.S. and Ph.D. degrees from the Georgia Institute of Technology, Atlanta, in 2001 and 2003, respectively, both in electrical engineering.

Since 2003, he has been an Assistant Professor in the Department of Electrical and Computer Engineering, Louisiana State University, Baton Rouge. His research interests are in image/video processing and computer vision. He has published more than 25

journal and conference papers. He is a member of the IEEE Signal Processing Society and SPIE.